Published in final edited form as:
Clin Cancer Res. 2015 November 15; 21(22): 5100–5109. doi:10.1158/1078-0432.CCR-15-0313.

Cyclin-dependent kinase inhibitor AT7519 as a potential drug for MYCN-dependent neuroblastoma

M. Emmy M. Dolman[1], **Evon Poon**[4], **Marli E. Ebus**[1], **Ilona J.M. den Hartog**[1], **Carel J.M. van Noesel**[2], **Yann Jamin**[5], **Albert Hallsworth**[4], **Simon P. Robinson**[5], **Kevin Petrie**[4], **Rolf W. Sparidans**[6], **Robbert J. Kok**[7], **Rogier Versteeg**[1], **Huib N. Caron**[3], **Louis Chesler**[4], and **Jan J. Molenaar**[1]

[1]Department of Oncogenomics, Academic Medical Center, University of Amsterdam, Amsterdam, the Netherlands [2]Department of Pathology, Academic Medical Center, University of Amsterdam, Amsterdam, the Netherlands [3]Department of Pediatric Oncology, Emma Kinderziekenhuis, Academic Medical Center, University of Amsterdam, Amsterdam, the Netherlands [4]Division of Clinical Studies, The Institute of Cancer Research, London, England [5]Division of Radiotherapy and Imaging, The Institute of Cancer Research, London, England [6]Division of Pharmacoepidemiology & Clinical Pharmacology, Utrecht Institute for Pharmaceutical Sciences (UIPS), Faculty of Science, Utrecht University, Utrecht, the Netherlands [7]Division of Pharmaceutics, Utrecht Institute for Pharmaceutical Sciences (UIPS), Faculty of Science, Utrecht University, Utrecht, the Netherlands

Abstract

Purpose—MYCN-dependent neuroblastomas have low cure rates with current multimodal treatment regimens and novel therapeutic drugs are therefore urgently needed. In previous pre-clinical studies we have shown that targeted inhibition of cyclin-dependent kinase 2 (CDK2) resulted in specific killing of *MYCN*-amplified neuroblastoma cells. This study describes the *in vivo* pre-clinical evaluation of the CDK inhibitor AT7519.

Experimental Design—Pre-clinical drug testing was performed using a panel of *MYCN*-amplified and *MYCN* single copy neuroblastoma cell lines and different MYCN-dependent mouse models of neuroblastoma.

Results—AT7519 killed *MYCN*-amplified neuroblastoma cell lines more potently than *MYCN* single copy cell lines with a median LC_{50} value of 1.7 compared to 8.1 μmol/L ($P = 0.0053$) and a significantly stronger induction of apoptosis. Preclinical studies in female NMRI homozygous (nu/nu) mice with neuroblastoma patient-derived *MYCN*-amplified AMC711T xenografts revealed dose-dependent growth inhibition, which correlated with intratumoural AT7519 levels. CDK2 target inhibition by AT7519 was confirmed by significant reductions in levels of phosphorylated retinoblastoma (p-Rb) and nucleophosmin (p-NPM). AT7519 treatment of *Th-*

Corresponding Author: M. Emmy M. Dolman, Department of Oncogenomics, Academic Medical Center, University of Amsterdam, Meibergdreef 15, PO Box 22700, 1105 AZ Amsterdam, the Netherlands. Phone number: +31-20-5665275; Fax: +31-20-6918626; memdolman@gmail.com.

Disclosure of Potential Conflicts of Interest
The authors declare no conflict of interest.

Europe PMC Funders Author Manuscripts

MYCN transgenic mice resulted in improved survival and clinically significant tumour regression (average tumour size reduction of 86% at day 7 after treatment initiation). The improved efficacy of AT7519 observed in *Th-MYCN* mice correlated with higher tumour exposure to the drug.

Conclusions—This study strongly suggests that AT7519 is a promising drug for the treatment of high-risk neuroblastoma patients with *MYCN* amplification.

Keywords

Neuroblastoma; *MYCN* amplification; CDK2 inhibition; AT7519; synthetic lethal

Introduction

Neuroblastoma are pediatric tumours that originate from the developing sympathetic nervous system. Current treatment regimens for high-risk tumours comprise a combination of high-dose cytostatics, radiation therapy, surgery, myeloablative therapy with stem cell reinfusion, long-term maintenance therapy with retinoic acid and immunotherapy using anti-disialoganglioside 2 antibodies. Despite this multimodal treatment strategy, the overall survival of high-risk neuroblastoma patients is still only below 50%. Especially patients with MYCN-dependent tumours have a very poor prognosis. Recent studies have shown that tumours with enhanced MYCN pathway activity not only include *MYCN*-amplified tumours, but also neuroblastoma tumours with *MYCN*-overexpression, implying that 50% of all high-risk neuroblastoma patients suffer from MYCN-dependent tumours (1).

Synthetic lethality has been widely explored as a mechanism to target oncogenic mutations, the clinical potential of which is exemplified by the use of poly ADP ribose polymerase (PARP) inhibitors in the treatment of tumours with mutated *BRCA* tumour suppressor genes (2-4). Synthetic lethality is particularly useful when the activity of a given oncoprotein cannot be directly targeted, as is the case with myelocytomatosis viral oncogene homolog (*MYC*) family of oncoproteins, (c-MYC, MYCN and MYCL). Screening efforts have led to the identification of aurora kinase B (*AURKB*), casein kinase 1 epsilon (*CSKN1E*), checkpoint kinases 1 and 2 (*CHEK1*, *CHEK2*), ataxia telangiectasia and Rad3 related (*ATR*) and several cyclin-dependent kinases (CDKs) as synthetic lethal with aberrant expression of MYC oncoproteins (5-8).

Previously, we described that silencing of CDK2 led to induction of apoptosis in neuroblastoma cells expressing high levels of MYCN (9). These findings were confirmed with the Cdc2/CDK2/CDK5 inhibitor roscovitine (Seliciclib), but unfavourable pharmacokinetic characteristics (i.e. short elimination half-life and rapid metabolic deactivation) (10, 11) led to failure to sufficiently inhibit CDK2 activity in neuroblastoma xenograft models. Recently, a number of clinical-candidate inhibitors that target CDK2 have been developed including BMS-387032 and AT7519, with IC_{50} values of 48 and 47 nM, respectively, for CDK2 (12, 13). In addition to CDK2, AT7519 also displays activity towards other CDKs (i.e. CDK1, CDK4, CDK5, CDK6 and CDK9 (as well as to a lesser extent CDK3 and CDK7 and glycogen synthase kinase 3 beta (GSK-3β)). AT7519 was identified by Astex using the Pyramid fragment-based drug discovery platform (13), and is the most extensively clinically evaluated inhibitor of CDK2. Currently, Phase II clinical trials of

Europe PMC Funders Author Manuscripts

Europe PMC Funders Author Manuscripts

AT7519 are ongoing for chronic lymphocytic leukemia, mantle cell lymphoma and multiple myeloma (http://clinicaltrials.gov), and our previous results suggested potential efficacy for the treatment of high-risk neuroblastoma. In the present study, we explored the potential of AT7519 for inhibiting MYCN-dependent neuroblastoma *in vitro* and *in vivo*.

Materials and Methods

Chemicals

AT7519 (>98%) was kindly provided by Astex. Etoposide, vincristine, cisplatin, topotecan, doxorubicin, irinotecan and temozolomide were purchased from Sigma Aldrich. For *in vivo* studies AT7519 was formulated in saline in final concentrations of 1.5 and 1.875 mg/mL.

Cell culture

Classical human neuroblastoma cell lines and neuroblastoma tumour-initiating cell (TIC) lines were cultured as previously described (14, 15). Cell culture protocols are described in detail in the Supplementary Materials and Methods.

IC_{50} and LC_{50}

Cells were seeded in triplicate in 96-well plates using the most optimal confluency for each cell line (Supplementary Table S1). Cells were incubated overnight and treated with 0.64 nmol/L – 10 μmol/L AT7519 using five-fold dilution steps. Control samples were treated with 0.1% DMSO. Cell viability was established prior to and at 72 h after treatment using the 3-(4,5-dimethylthiazol-2-yl)-2,5-diphenyltetrazolium bromide (MTT) colorimetric assay (16). Half maximal effective concentration (IC_{50}) and half lethal concentration (LC_{50}) values were derived from dose-response curves. IC_{50} values at 72 h were calculated by determining the AT7519 concentrations needed to achieve a 50% reduction in cell viability observed for DMSO-treated cells at 72 h (set at 100%). LC_{50} values at 72 h were calculated by determining the AT7519 concentrations needed to achieve a 50% reduction in the cell viability at 0 h.

Western Blotting

The following antibodies were used: mouse anti-human Rb (clone G3-245) monoclonal antibody (1:1000, BD Biosciences); rabbit anti-human p-Rb (Thr^{821}) polyclonal antibody (1:1000, BioSource International); mouse anti-human MYCN (clone B8.4.B) monoclonal antibody (1:5000, BD Biosciences); rabbit anti-human PARP polyclonal antibody (1:2000, Cell Signaling Technology); rabbit anti-human NPM polyclonal antibody (1:1000, Cell Signaling Technology); rabbit anti-human p-NPM (Thr199) polyclonal antibody (1:500, Cell Signaling Technology); rabbit anti-human β-actin (clone 13E5) monoclonal antibody (1:1000, Cell Signaling Technology); mouse anti-human β-actin (clone AC-15) monoclonal antibody (1:20000, Abcam); mouse anti-human α-tubulin (clone DM1A) monoclonal antibody (1:1000, Cell Signaling Technology) and IRDye 800CW goat anti-rabbit and goat anti-mouse secondary antibodies (1:5000, Li-COR). See Supplementary Materials and Methods for a detailed protocol.

Europe PMC Funders Author Manuscripts

Immunohistochemistry

The following antibodies were used: rabbit anti-human NPM polyclonal antibody (1:1000, Cell Signaling Technology); rabbit anti-human p-NPM (Thr199) polyclonal antibody (1:400, Cell Signaling Technology); rabbit anti-human Ki-67 (clone SP6) monoclonal antibody (1:1000, Thermo Scientific), rabbit anti-human cleaved caspase 3 (Asp175) polyclonal antibody (1:100, Cell Signaling Technology) and BrightVision horseradish peroxidase-conjugated goat anti-rabbit polyclonal secondary antibody (undiluted; 30 min; Immunologic). See Supplementary Materials and Methods for a detailed protocol.

FACS analysis

Cells were treated with 0.1% DMSO (control), 150 nmol/L AT7519 (100 nmol/L for IMR32) or AT7519 concentrations equal to the IC_{50} for each individual cell line (see Supplementary Table S1 for the IC_{50} values). After 72 h treatment, floating and adherent cells were harvested for FACS analysis to determine the cell cycle distribution and the apoptotic sub-G1 fraction. See Supplementary Materials and Methods for a detailed protocol.

In vivo efficacy in neuroblastoma xenograft mouse models

Female NMRI nu/nu mice (6-15 weeks old; 20-30 g) were obtained from Harlan and experiments were performed with permission from and according to the standards of the Dutch animal ethics committee (DEC 102389 and 102690). NMRI nu/nu mice were subcutaneously injected with 1-5 × 10^6 cells/flank of AMC711T or KCNR. The size of the tumours was recorded twice weekly and when tumours reached a size of approximately 1000 mm^3, tumour pieces were serially xenotransplanted in recipient mice. Parts of the xenotransplanted tumours were formalin-fixed and paraffin-embedded sections were routinely checked by haematoxylin-eosin staining. For the *in vivo* efficacy studies, recipient mice with AMC711T or KCNR neuroblastoma xenografts with a mean volume of 268 mm^3 were subsequently treated intraperitoneally (i.p.) with 5, 10 or 15 mg/kg/day AT7519 or vehicle (saline) in a five days on, two days off schedule for up to three weeks consecutively. Tumour sizes were measured by an external calliper.

In vivo efficacy in *Th-MYCN* transgenic mice

All experimental protocols were monitored and approved by The Institute of Cancer Research Animal Welfare and Ethical Review Body, in compliance with guidelines specified by the UK Home Office Animals (Scientific Procedures) Act 1986 and the United Kingdom National Cancer Research Institute guidelines for the welfare of animals in cancer research (17) and ARRIVE guidelines (18). In *Th-MYCN* mice (129X1/SvJ-Tg(Th-MYCN)41Waw/Nci), expression of a human *MYCN* transgene is directed by a rat tyrosine hydrolase (Th) promoter to neural crest cells during early development (19). *Th-MYCN* mice were genotyped to detect the presence of human *MYCN* transgene. After weaning, animals were palpated for intra-abdominal tumours twice weekly. Mice (40–80 days old) with palpable tumours (mean size of 960 mm^3) were randomized and treated i.p. with 15 mg/kg/day AT7519 or vehicle (saline) in a five days on, two days off schedule for up to three weeks consecutively. Tumour volume was determined by MRI on a 7T horizontal bore

microimaging system (Bruker Instruments) using a 3 cm birdcage coil. Anatomical T2-weighted coronal images were acquired from 20 contiguous 1-mm-thick slices through the mouse abdomen, from which tumour volumes were determined using segmentation from regions of interest drawn on each tumour-containing slice. Mice were allowed access to food and water *ad libitum*.

In vivo pharmacokinetics

Mice with AMC711T neuroblastoma xenografts (~268 mm^3) were treated with a single i.p. injection of 5, 10 or 15 mg/kg AT7519 or saline. Blood samples were collected by cheek puncture (t = 1 min) or from the posterior vena cava (other time points) up to 24 h after administration. Plasma samples were obtained by centrifugation twice at 1150×*g* for 15 min. Tumour samples were homogenized in saline in a final concentration of 0.1 g/mL using the Precellys 24-Dual. Samples were stored at −80°C until pre-treatment and analysis by LC-MS/MS as described for plasma by Dolman *et al.* (20). Pharmacokinetic parameters were calculated by fitting to a first-order two-compartment model with Multifit pharmacokinetic software (Dr. Hans Proost, University of Groningen, the Netherlands). *Th-MYCN* transgenic mice (~960 mm^3) and mice with KCNR neuroblastoma xenografts (~268 mm^3) were treated with a single i.p. injection of 15 mg/kg AT7519 or saline. Blood and tumour samples were collected at 1 hr and 4 h after AT7519 administration and processed and analyzed as described above.

In vivo pharmacodynamics

Mice with AMC711T neuroblastoma xenografts (~268 mm^3) were treated with a daily i.p. injection of 5, 10 or 15 mg/kg AT7519 or saline for five consecutive days. Tumour material was collected at 1 h after administration of the last dose and skin biopsies were taken prior to treatment and at 1 h after the last dose. For *Th-MYCN* transgenic mice, mice were five days treated with 15 mg/kg/day AT7519 and tumour material was collected at 6 h after administration of the last dose.

Results

Neuroblastoma cells with *MYCN* amplification are sensitized to AT7519 treatment

The efficacy of AT7519 was evaluated in a panel of 20 *MYCN*-amplified and 9 non-*MYCN*-amplified cell lines using the MTT cell viability assay (Supplementary Fig. S1A and Supplementary Table S1). *MYCN*-amplified neuroblastoma cell lines were found to be significantly more sensitive to AT7519 compared with non-*MYCN*-amplified cell lines, as was demonstrated by the median IC_{50} values of 386 nmol/L and 1227 nmol/L ($P = 0.0074$), respectively (Fig. 1). Differences in sensitivity became more obvious when taking the induction of cell death into account by means of the LC_{50} values (Fig. 1). Less overlap was observed between the LC_{50} values obtained in *MYCN*-amplified and non-*MYCN*-amplified neuroblastoma cell lines, with median LC_{50} values of 1.7 and 8.1 μmol/L ($P = 0.0053$), respectively. The sensitivity of neuroblastoma cell lines to AT7519 did not correlate with *MYCN* mRNA (Supplementary Fig. S1B) or MYCN protein levels (Supplementary Fig. S1C), indicating that the presence of *MYCN* amplification is the best predictive biomarker for AT7519 efficacy.

Next we treated *MYCN*-amplified and non-*MYCN*-amplified cell lines with increasing doses of AT7519 to study effects on retinoblastoma protein (Rb) phosphorylation (p-Rb) and PARP cleavage. Rb is a direct target of CDK2, activated by phosphorylation on threonine 821 (Thr^{821}). AT7519 treatment led to a dose-dependent diminution of p-Rb levels, independent of *MYCN* status (Fig. 2A). But p-Rb inhibition in *MYCN*-amplified neuroblastoma cell lines resulted in more potent PARP cleavage induction than observed for non-*MYCN*-amplified cell lines. Treatment of *MYCN*-amplified cell lines with IC_{25}, IC_{50} or IC_{75} concentrations of AT7519 resulted in average increases in PARP cleavage of 1.1%, 7.6% and 14.1%, respectively, versus 0.4, 2.1 and 1.9% for non-*MYCN*-amplified cell lines (Fig.2A and Supplementary Fig. S2). In some neuroblastoma cell lines, total Rb and/or MYCN protein levels were inhibited at higher concentrations of AT7519 treatment. This may relate to additional inhibitory activities of the compound.

The apoptotic effects of AT7519 were further studied by flow cytometry after treatment with AT7519 concentrations equal to 150 nmol/L or the IC_{50} for each individual cell line (Supplementary Fig. S3). For 7 out of 9 *MYCN*-amplified neuroblastoma cell lines treated with 150 nmol/L AT7519 larger increases in sub-G1 fraction were observed than for non-*MYCN*-amplified cell lines, with average increases in sub-G1 fraction of 12.4% and 0.6%, respectively (Fig. 2B and Supplementary Table S2). As expected, treatment with the IC_{50} dose of AT7519 resulted in a greater sub-G1 population in all *MYCN*-amplified cell lines for which the IC_{50} was > 150 nmol/L. In contrast, no significant increases in sub-G1 fraction were observed for 2 out of 4 non-*MYCN*-amplified cell lines (i.e. SKNSH and SY5Y), despite of treatment with micromolar concentrations of AT7519. Instead, high AT7519 doses caused G1 arrest of SKNSH and SY5Y. Together, these findings indicate that AT7519 treatment leads to a more pronounced apoptotic response in *MYCN*-amplified neuroblastoma cells, thereby confirming the differences in sensitivity between *MYCN*-amplified and non-*MYCN*-amplified cell lines shown in Fig. 1.

For the clinical implementation of AT7519 it is also important to establish whether or not AT7519 can be combined with drugs that are conventionally used for neuroblastoma treatment. We therefore performed *in vitro* combination studies with the *MYCN*-amplified neuroblastoma cell lines IMR32 and NGP, in which effects on cell viability were studied. AT7519 was combined with ciplatin, doxorubicin, irinotecan, temozolomide, topotecan, vincristine or etoposide. While AT7519 did not display synergistic effects with any of the standard cytostatic drugs evaluated in either IMR32 or NGP cells, no antagonism was observed (Supplementary Fig. S4).

AT7519 inhibits the growth of MYCN-amplified neuroblastoma xenografts

The efficacy of AT7519 was subsequently studied *in vivo* in mice with MYCN-amplified AMC711T neuroblastoma xenografts. AMC711T cells are short-term cultured primary neuroblastoma cells and xenografts of these cells have shown to properly reflect high-risk neuroblastoma (14). Mice were treated daily with i.p. injections of 5, 10 or 15 mg/kg AT7519 in a 5-days on, 2-days off schedule for three weeks consecutively. AT7519 inhibited the growth of AMC711T neuroblastoma xenografts in a dose-dependent manner, with even the lowest dose of 5 mg/kg providing a statistically significant reduction in tumour growth

(Fig. 3A and Supplementary Fig. S5A). Treatment with either 10 or 15 mg/kg AT7519 almost completely blocked tumour growth, resulting in a significantly improved anticancer effect compared with 5 mg/kg AT7519 (Fig. 3A). More rapid tumour growth was observed after terminating treatment with AT7519 (Supplementary Fig. S5B). We also tested AT7519 (15 mg/kg) in *MYCN*-amplified KCNR neuroblastoma xenografts and found a 50% reduction in tumour growth compared to saline control at day 17 after treatment initiation (Supplementary Fig. S5C).

In vivo efficacy of AT7519 correlates with tumour drug exposure

To further evaluate the tumour-specific effects of AT7519, intratumoural and plasma drug concentrations were correlated with the dose-dependent tumour growth inhibitory effects in AMC711T xenografts. AT7519 concentrations in plasma and tumour were measured up to 24 h after i.p administration of a single dose of 5, 10 or 15 mg/kg AT7519. Plasma clearance and tumour accumulation curves were fitted for each individual dose (Fig. 3B and Supplementary Fig. S5D) and fitted curves were used to calculate pharmacokinetic parameters (Supplementary Table S3). No AT7519 could be detected in plasma or tumour 24 h after administration of the compound regardless of dose. AT7519 rapidly entered the circulation from the peritoneal cavity, as demonstrated by the short time needed to reach maximum plasma levels (T_{max} <7 min). Plasma $AUC_{0-\infty}$ values correlated with AT7519 doses (Fig. 3C), such that the biological availability after i.p. administration of AT7519 was equivalent for all three doses evaluated. When comparing the maximum AT7519 plasma levels (C_{max}), no increase in C_{max} was observed after administration of 15 mg/kg AT7519. Also a slightly longer plasma terminal half-life was observed with 15 mg/kg AT7519 compared with the lower doses (Supplementary Table S3). These observations indicate a slight change in pharmacokinetic behaviour, potentially due to partial precipitation of AT7519 in the peritoneal cavity. Gradual redissolution of AT7519 might eventually lead to the same biological availability as observed for the lower doses.

AT7519 rapidly entered the tumours (Fig. 3B, Supplementary Fig. S5D and Supplementary Table S3), with maximum intratumoural drug concentrations reached within 25-40 min after AT7519 administration. Maximum intratumoural AT7519 concentrations linearly increased with increasing dose. However, as shown by the tumour $AUC_{0-\infty}$ values, administration of 15 mg/kg AT7519 did not result in a linear increase in tumour exposure to the inhibitor (Fig. 3C and Supplementary Table S3). This might explain why treatment of AMC711T neuroblastoma xenografts with 15 mg/kg/day AT7519 did not result in significantly improved efficacy as compared with 10 mg/kg/day AT7519. Independent of dose, AT7519 was eliminated from the tumour with a terminal half-life of approximately 1.8 h. The results obtained with AMC711T neuroblastoma xenografts were reproduced with KCNR xenografts (15 mg/kg), with plasma and intratumoral AT7519 levels detected at 1 and 4 h after administration of a single i.p. injection (Supplementary Fig. S5E). Taken together, these observations show that the efficacy of AT7519 correlates to the overall tumour exposure to AT7519.

Loss of Rb and NPM phosphorylation are biomarkers for AT7519 efficacy in MYCN-driven tumours

Because Rb and nucleophosmin (NPM) are direct targets for phosphorylation by CDK2, we investigated the use of p-Rb and p-NPM as potential biomarkers of AT7519 efficacy. Mice bearing AMC711T neuroblastoma xenografts were treated with 5, 10 or 15 mg/kg/day AT7519 for five consecutive days. Inhibitory effects of AT7519 on tumoural p-Rb and p-NPM levels were evaluated 1 h after administration of the last dose. AT7519 significantly reduced tumour levels of p-Rb and p-NPM, despite inter-animal variation (Fig. 3D and E and Supplementary Fig. S6A). Furthermore, treatment with either 10 or 15 mg/kg/day AT7519 resulted in decreased levels of p-Rb and p-NPM compared to 5 mg/kg/day AT7519. Inhibitory effects on phosphorylated NPM levels were also studied *in situ* (Fig. 3F and Supplementary Fig. S6B). Again, significant inhibition of p-NPM was observed, even after treatment with 5 mg/kg/day AT7519. No effects of AT7519 on total NPM levels were observed (Supplementary Fig. S6A and B). Hematoxylin-eosin staining of the tumour tissues did not indicate clear phenotypic changes between vehicle and AT7519 treated mice (Supplementary Fig. S6C).

AT7519 causes tumour volume reduction in *Th-MYCN* transgenic mice

Given that *Th-MYCN* transgenic mice develop tumours in an immunocompetent background, we reasoned that the preclincal evaluation of AT7519 in this mouse model would be complementary to our xenograft data. Consistent with both neuroblastoma xenograft models tested, *Th-MYCN* transgenic mice were treated with 15 mg/kg/day AT7519 in a 5-days on, 2-days off schedule for three weeks consecutively. Magnetic resonance imaging at day 7 after treatment initiation with AT7519 showed significant reductions in tumour volume (Fig. 4A and Supplementary Fig. S7A). Tumour volume reduction was observed for all treated mice, with 6/7 partial responses (PR; i.e. 50-95% tumour volume reduction) and 1/7 very good partial response (VGPR; i.e. 95-99.99% tumour volume reduction) (Fig. 4B). The average reduction in tumour volume was approximately 86% at day 7 after treatment initiation with AT7519. In contrast, all saline treated mice showed progressive disease (PD), with an average increase in tumour volume of approximately 218% (Fig. 4B and Supplementary Fig. S7A). Three weeks treatment with AT7519 significantly increased the overall survival of *Th-MYCN* transgenic mice (Fig. 4C). However, consistent with tumour regrowth observed for our neuroblastoma xenograft studies, *Th-MYCN* mice relapsed while on AT7519 treatment (Supplementary Fig. S7B and C).

Unexpectedly, intratumoural concentrations of AT7519 at 1 h after a single i.p. injection of 15 mg/kg were almost three times higher than the predicted levels based on the xenograft models, while average plasma levels were approximately 40% lower (Fig. 4D). This corresponds with an approximately 5-fold higher tumour/plasma ratio for the *Th-MYCN* transgenic mouse model. No differences in observed and predicted plasma and intratumoural AT7519 levels were observed at 4 h after administration of AT7519. Thus the tumour exposure to AT7519 is higher for the *Th-MYCN* transgenic mouse model than both neuroblastoma xenograft models tested in this study. This might explain the improved efficacy of AT7519 observed for *Th-MYCN* transgenic mice.

Pharmacodynamic analysis showed that AT7519 strongly induced cell death in *Th-MYCN* tumours. Treatment of these mice with 15 mg/kg/day AT7519 resulted in increased cleavage of caspase 3 (Fig. 5A and Supplementary Fig. S8A and B) and the occurrence of nuclear condensation and fragmentation and necrosis (Fig. 5B). Effects on apoptosis after AT7519 treatment of *Th-MYCN* transgenic mice were consistent with the observed tumour regression.

Discussion

The work presented here describes the preclinical evaluation of the novel fragment-derived small molecule CDK inhibitor AT7519 in neuroblastoma treatment. In agreement with our previous results, the sensitivity of neuroblastoma cells to AT7519 partly depends on the *MYCN* amplification status. The degree to which AT7519 specifically killed cells with *MYCN* amplification versus non-*MYCN*-amplified cells, however, was less pronounced than the synthetic lethal interaction between knockdown of *CDK2* and *MYCN* amplification (9). The underlying reason for this is likely that while AT7519 was originally described as a unique CDK2 inhibitor that binds within the active site cleft of CDK2 overlapping with the ATP-binding pocket (13), it also effectively targets additional kinases including CDK1, CDK4, CDK5, CDK6 and CDK9 (IC_{50} values of 210-220 nM, 67-100 nM, 11-13 nM, 170 nM and <10-100 nM, respectively) and to a lesser extent CDK3 and CDK7 (21, 22). The sensitivity of neuroblastoma cells to AT7519 did not correlate with *MYCN* mRNA or MYCN protein levels, but the high expression of c-MYC and MYCN in neuroblastoma cell lines SJNB12 and SJNB1, respectively, might explain why these non-*MYCN*-amplified cell lines were more sensitive to AT7519 than the other non-*MYCN*-amplified cell lines.

AT7519 caused loss of phosphorylated Rb in all neuroblastoma cell lines studied, independent of *MYCN* status. In some cell lines, however, p-Rb inhibition was only observed after treatment with IC_{75} instead of IC_{50} doses of AT7519, indicating the involvement of other mechanisms than CDK2 inhibition in the anticancer activity of AT7519 in neuroblastoma cells. In addition, high dose treatment with AT7519 elicited striking down-regulation of MYCN protein levels in the majority of *MYCN*-amplified neuroblastoma cell lines. This finding is consistent with roscovitine and its derivative CR8, both of which have been shown to down-regulate MYCN expression in *MYCN*-amplified neuroblastoma cell lines via RNA polymerase II deactivation through inhibition of CDK7, CDK 9 and CDK12 (23). Thus the inhibitory activity of AT7519 towards CDK9 may explain the loss of MYCN expression observed in our current study. The observation that effects on MYCN do not correlate with effects on Rb phosphorylation supports that AT7519-induced MYCN loss is CDK2-independent. However, it is noteworthy that in most cases PARP cleavage occurred with AT7519 doses insufficient to promote depletion of MYCN. This, together with the observation that only limited PARP cleavage induction was observed in non-*MYCN*-amplified neuroblastoma cell lines after AT7519 treatment argues for MYCN-dependency of AT7519-induced apoptosis.

In this study we used both xenograft models and a genetically engineered model (GEM) to evaluate AT7519 preclinically. The use of patient-derived short-term cultured lines such as the *MYCN*-amplified neuroblastoma TIC line AMC711T (14) is an important step forward

in the development of *in vivo* xenograft models of neuroblastoma. However, xenograft models still have the principal drawback that they lack an intact immune system (24). We therefore complemented our xenograft studies with the immunocompetent *Th-MYCN* GEM model. *Th-MYCN* mice express MYCN in the developing neural crest, leading to the spontaneous development of neuroblastoma tumours (24, 25). Treatment with AT7519 resulted in a more potent anticancer activity in *Th-MYCN* transgenic mice compared with the anticancer effects obtained in the AMC711T and KCNR xenograft models. Our data suggest that this may be caused by an increased tumour exposure to AT7519 in *Th-MYCN* transgenic mice, which might be the result of a higher degree of tumour vascularisation. There are indications that MYCN promotes tumour angiogenesis (26) and recent functional MRI and histopathological studies demonstrated that *Th-MYCN* tumours display a high degree of perfusion (i.e. almost 20%) compared to subcutaneous xenografts differentially expressing MYCN (i.e. ~ 5%) (27, 28). *Th-MYCN* tumours also exhibit a high degree of vessel permeability, facilitating the delivery of drugs to the tumour side (29). These characteristics may also explain the more rapid clearance of AT7519 from *Th-MYCN* tumours whereby intratumoural AT7519 concentrations dropped to the same level at 4 h after drug administration as observed in both xenograft models. Differences in tumour localisation might also contribute to the variability in intratumoural drug levels. While neuroblastoma xenografts are localised subcutaneously at the rear flanks, tumours in *Th-MYCN* transgenic mice develop in the paraspinal ganglia (25). Tumours derived in *Th-MYCN* transgenic mice are therefore localised closer to the injection site of AT7519.

The pharmacokinetic properties of AT7519 reported here are in line with a previous study with mice bearing HCT116 colon cancer xenografts (21). Mice treated with 5 mg/kg AT7519 administered intravenously (i.v.) displayed a plasma C_{max} and $t_{1/2}$ of 1750 ng/mL and 1.1 h, respectively, which is in the same order of magnitude as the plasma C_{max} and $t_{1/2}$ found in this study after i.p. administration of AT7519 (i.e. 1886 ng/mL and 1.6 h, respectively). Also the plasma $AUC_{0-\infty}$ values are comparable, i.e. 1628 h*ng/mL (i.p) versus 1513 h*ng/mL (i.v.), indicating a 100% biological availability after i.p. administration of AT7519. Looking at the tumour distribution of AT7519, we found a slightly higher C_{max} in our neuroblastoma xenografts, i.e. 958 ng/g versus 684 ng/mL after i.v. administration to mice bearing HCT116 colon cancer xenografts (assuming 1 mL tissue=1 g tissue). The tumour AT7519 exposure after i.p. administration in our study was however almost equal to the exposure observed by Squires *et al.* after i.v. administration to mice with colon cancer xenografts, as demonstrated by the tumour $AUC_{0-\infty}$ values of, respectively, 3069 h*ng/g and 3015 h*ng/mL. This might be explained by the slightly shorter tumour $t_{1/2}$ observed for the AMC711T neuroblastoma xenografts (21).

Interpatient variability in drug pharmacokinetics and pharmacodynamics is a well-known phenomenon in the clinical treatment of cancer patients (30). It is therefore important to be able to establish if neuroblastoma patients receive an appropriate AT7519 dose and whether or not AT7519 exerts its desired effects. Based on intratumoural AT7519 concentrations, drug dosage adjustments can be performed to compensate for the interpatient variability in drug pharmacokinetics. This study also demonstrated that loss of phosphorylation of the direct CDK2 targets Rb and NPM can be utilized as target-specific efficacy biomarkers of AT7519. Loss of both p-Rb and p-NPM biomarkers was observed after AT7519 treatment in

mice bearing AMC711T neuroblastoma xenografts. Inhibitory effects on p-Rb and p-NPM also seemed to be higher after treatment with 10 or 15 mg/kg/day AT7519 than after treatment with 5 mg/kg/day of the CDK2 inhibitor. These findings are consistent with results obtained clinically in human promyelocytic leukemia xenografts, where treatment with AT7519 also resulted in inhibition of tumour-associated p-Rb and p-NPM (31). In the *Th-MYCN* model we saw that treatment with 15 mg/kg/day AT7519 caused an increase in cleaved caspase 3. Additional studies are needed to validate if this apoptotic marker can be used as non-target-specific biomarker of efficacy of AT7519.

The clinical use of AT7519 has been associated with dose-limiting toxicities, including QTc prolongation (22). However, follow-up studies showed that treating patients at days 1, 4, 8 and 11 once every 3 weeks instead of at days 1-5 appears to limit the risk of QTc prolongation (32). Currently running clinical trials with AT7519 are therefore performed using the new intermittend treatment schedule (https://clinicaltrials.gov).

Taken together, the results presented in this study strongly suggest that AT7519 is a clinical candidate drug for the treatment of *MYCN*-amplified, high-risk neuroblastoma. The ability of AT7519 to rapidly decrease tumour volume in *Th-MYCN* mice indicates its possible use in the induction phase of treatment. Finally, the potential utility of AT7519 is increased by the identification of target-specific efficacy biomarkers.

Supplementary Material

Refer to Web version on PubMed Central for supplementary material.

Acknowledgments

Grant Support

The research in this paper was supported by grants from Villa Joep, Tom Voûte Fund, KiKa, Christopher's Smile Charity (CXC001 and CXC002X), Felix White Charity (RFR065X), Cancer Research UK and EPSRC to the Cancer Imaging Centre at ICR and RMH, in association with the MRC and Department of Health (England) (C1060/A10334 and C1060/A16464), the Wellcome Trust (091763Z/10/Z), an EPSRC Platform Grant (EP/H046526/1), NHS funding to the NIHR Biomedical Research Centre, and a Paul O'Gorman Postdoctoral Fellowship funded by Children with Cancer UK.

References

1. Valentijn LJ, Koster J, Haneveld F, Aissa RA, van Sluis P, Broekmans ME, et al. Functional *MYCN* signature predicts outcome of neuroblastoma irrespective of *MYCN* amplification. Proc Natl Acad Sci U S A. 2012; 109(47):19190–5. [PubMed: 23091029]
2. Chan DA, Giaccia AJ. Harnessing synthetic lethal interactions in anticancer drug discovery. Nat Rev Drug Discov. 2011; 10(5):351–64. [PubMed: 21532565]
3. Kaelin WG Jr. The concept of synthetic lethality in the context of anticancer therapy. Nat Rev Cancer. 2005; 5(9):689–98. [PubMed: 16110319]
4. Fong PC, Boss DS, Yap TA, Tutt A, Wu P, Mergui-Roelvink M, et al. Inhibition of poly(ADP-ribose) polymerase in tumors from BRCA mutation carriers. N Engl J Med. 2009; 361(2):123–34. [PubMed: 19553641]
5. Murga M, Campaner S, Lopez-Contreras AJ, Toledo LI, Soria R, Montana MF, et al. Exploiting oncogene-induced replicative stress for the selective killing of Myc-driven tumors. Nat Struct Mol Biol. 2011; 18(12):1331–5. [PubMed: 22120667]

6. Cole KA, Huggins J, Laquaglia M, Hulderman CE, Russell MR, Bosse K, et al. RNAi screen of the protein kinome identifies checkpoint kinase 1 (CHK1) as a therapeutic target in neuroblastoma. Proc Natl Acad Sci U S A. 2011; 108(8):3336–41. [PubMed: 21289283]
7. Toyoshima M, Howie HL, Imakura M, Walsh RM, Annis JE, Chang AN, et al. Functional genomics identifies therapeutic targets for MYC-driven cancer. Proc Natl Acad Sci U S A. 2012; 109(24): 9545–50. [PubMed: 22623531]
8. Yang D, Liu H, Goga A, Kim S, Yuneva M, Bishop JM. Therapeutic potential of a synthetic lethal interaction between the MYC proto-oncogene and inhibition of aurora-B kinase. Proc Natl Acad Sci U S A. 2010; 107(31):13836–41. [PubMed: 20643922]
9. Molenaar JJ, Ebus ME, Geerts D, Koster J, Lamers F, Valentijn LJ, et al. Inactivation of CDK2 is synthetically lethal to *MYCN* over-expressing cancer cells. Proc Natl Acad Sci U S A. 2009; 106(31):12968–73. [PubMed: 19525400]
10. Sallam H, El-Serafi I, Meijer L, Hassan M. Pharmacokinetics and biodistribution of the cyclin-dependent kinase inhibitor -CR8- in mice. BMC Pharmacol Toxicol. 2013; 14:50. [PubMed: 24079553]
11. Nutley BP, Raynaud FI, Wilson SC, Fischer PM, Hayes A, Goddard PM, et al. Metabolism and pharmacokinetics of the cyclin-dependent kinase inhibitor R-roscovitine in the mouse. Mol Cancer Ther. 2005; 4(1):125–39. [PubMed: 15657360]
12. Misra RN, Xiao HY, Kim KS, Lu S, Han WC, Barbosa SA, et al. N-(cycloalkylamino)acyl-2-aminothiazole inhibitors of cyclin-dependent kinase 2. N-[5-[[[5-(1,1-dimethylethyl)-2-oxazolyl]methyl]thio]-2-thiazolyl]-4- piperidinecarboxamide (BMS-387032), a highly efficacious and selective antitumor agent. J Med Chem. 2004; 47(7):1719–28. [PubMed: 15027863]
13. Wyatt PG, Woodhead AJ, Berdini V, Boulstridge JA, Carr MG, Cross DM, et al. Identification of N-(4-piperidinyl)-4-(2,6-dichlorobenzoylamino)-1H-pyrazole-3-carboxamide (AT7519), a novel cyclin dependent kinase inhibitor using fragment-based X-ray crystallography and structure based drug design. J Med Chem. 2008; 51(16):4986–99. [PubMed: 18656911]
14. Bate-Eya LT, Ebus ME, Koster J, den Hartog IJ, Zwijnenburg DA, Schild L, et al. Newly-derived neuroblastoma cell lines propagated in serum-free media recapitulate the genotype and phenotype of primary neuroblastoma tumours. Eur J Cancer. 2014; 50(3):628–37. [PubMed: 24321263]
15. Lamers F, Schild L, Koster J, Versteeg R, Caron HN, Molenaar JJ. Targeted BIRC5 silencing using YM155 causes cell death in neuroblastoma cells with low ABCB1 expression. Eur J Cancer. 2012; 48(5):763–71. [PubMed: 22088485]
16. Twentyman PR, Luscombe M. A study of some variables in a tetrazolium dye (MTT) based assay for cell growth and chemosensitivity. Br J Cancer. 1987; 56(3):279–85. [PubMed: 3663476]
17. Workman P, Aboagye EO, Balkwill F, Balmain A, Bruder G, Chaplin DJ, et al. Guidelines for the welfare and use of animals in cancer research. Br J Cancer. 2010; 102(11):1555–77. [PubMed: 20502460]
18. Kilkenny C, Browne WJ, Cuthill IC, Emerson M, Altman DG. Improving bioscience research reporting: the ARRIVE guidelines for reporting animal research. PLoS Biol. 2010; 8(6):e1000412. [PubMed: 20613859]
19. Weiss WA, Aldape K, Mohapatra G, Feuerstein BG, Bishop JM. Targeted expression of MYCN causes neuroblastoma in transgenic mice. EMBO J. 1997; 16(11):2985–95. [PubMed: 9214616]
20. Dolman MEM, den Hartog IJM, Molenaar JJ, Schellens JHM, Beijnen JH, Sparidans RW. Liquid chromatography-tandem mass spectrometric assay for the cyclin-dependent kinase inhibitor AT7519 in mouse plasma. Journal of Pharmaceutical and Biomedical Analysis. 2014; 88(0):216–20. [PubMed: 24080524]
21. Squires MS, Feltell RE, Wallis NG, Lewis EJ, Smith DM, Cross DM, et al. Biological characterization of AT7519, a small-molecule inhibitor of cyclin-dependent kinases, in human tumor cell lines. Mol Cancer Ther. 2009; 8(2):324–32. [PubMed: 19174555]
22. Mahadevan D, Plummer R, Squires MS, Rensvold D, Kurtin S, Pretzinger C, et al. A phase I pharmacokinetic and pharmacodynamic study of AT7519, a cyclin-dependent kinase inhibitor in patients with refractory solid tumors. Ann Oncol. 2011; 22(9):2137–43. [PubMed: 21325451]

23. Delehouze C, Godl K, Loaec N, Bruyere C, Desban N, Oumata N, et al. CDK/CK1 inhibitors roscovitine and CR8 downregulate amplified *MYCN* in neuroblastoma cells. Oncogene. 2013 DOI: 10.1038/onc.2013.513.
24. Quarta C, Cantelli E, Nanni C, Ambrosini V, D'Ambrosio D, Di Leo K, et al. Molecular imaging of neuroblastoma progression in *Th-MYCN* transgenic mice. Mol Imaging Biol. 2013; 15(2):194–202. [PubMed: 22777578]
25. Teitz T, Stanke JJ, Federico S, Bradley CL, Brennan R, Zhang J, et al. Preclinical models for neuroblastoma: establishing a baseline for treatment. PLoS One. 2011; 6(4):e19133. [PubMed: 21559450]
26. Chanthery YH, Gustafson WC, Itsara M, Persson A, Hackett CS, Grimmer M, et al. Paracrine signaling through *MYCN* enhances tumor-vascular interactions in neuroblastoma. Sci Transl Med. 2012; 4(115):115ra3.
27. Jamin Y, Tucker ER, Poon E, Popov S, Vaughan L, Boult JK, et al. Evaluation of clinically translatable MR imaging biomarkers of therapeutic response in the TH-MYCN transgenic mouse model of neuroblastoma. Radiology. 2013; 266(1):130–40. [PubMed: 23169794]
28. Calero R, Morchon E, Johnsen JI, Serrano R. Sunitinib suppress neuroblastoma growth through degradation of MYCN and inhibition of angiogenesis. PLoS One. 2014; 9(4):e95628. [PubMed: 24759734]
29. Jamin Y, Glass L, Hallsworth A, George R, Koh DM, Pearson AD, et al. Intrinsic susceptibility MRI identifies tumors with ALKF1174L mutation in genetically-engineered murine models of high-risk neuroblastoma. PLoS One. 2014; 9(3):e92886. [PubMed: 24667968]
30. Schell RF, Sidone BJ, Caron WP, Walsh MD, White TF, Zamboni BA, et al. Meta-analysis of inter-patient pharmacokinetic variability of liposomal and non-liposomal anticancer agents. Nanomedicine. 2014; 10(1):109–17. [PubMed: 23891988]
31. Squires MS, Cooke L, Lock V, Qi W, Lewis EJ, Thompson NT, et al. AT7519, a cyclin-dependent kinase inhibitor, exerts its effects by transcriptional inhibition in leukemia cell lines and patient samples. Mol Cancer Ther. 2010; 9(4):920–8. [PubMed: 20354122]
32. Chen EX, Hotte S, Hirte H, Siu LL, Lyons J, Squires M, et al. A Phase I study of cyclin-dependent kinase inhibitor, AT7519, in patients with advanced cancer: NCIC Clinical Trials Group IND 177. Br J Cancer. 2014; 111(12):2262–7. [PubMed: 25393368]

Europe PMC Funders Author Manuscripts

Europe PMC Funders Author Manuscripts

Statement of translational relevance

Novel drugs for patients with *MYCN*-amplified neuroblastoma are urgently needed. Given that direct inhibitors of MYCN oncoprotein are not yet available, the identification and validation of novel synthetic lethal interactors with MYCN is crucial. The current study describes the preclinical evaluation of AT7519, a novel inhibitor of cyclin-dependent kinases (CDK) including CDK2. AT7519 kills *MYCN*-amplified neuroblastoma cells with greater potency compared to those without *MYCN* amplification. Furthermore, AT7519 elicited striking anticancer effects in different *in vivo* models of *MYCN*-amplified neuroblastoma. Tumour responses correlated well with the AT7519 exposure and effects on pharmacodynamic biomarkers of AT7519 efficacy. Taken together, these results suggest that AT7519 is a promising clinical drug for the treatment of children with high-risk, *MYCN*-amplified neuroblastoma.

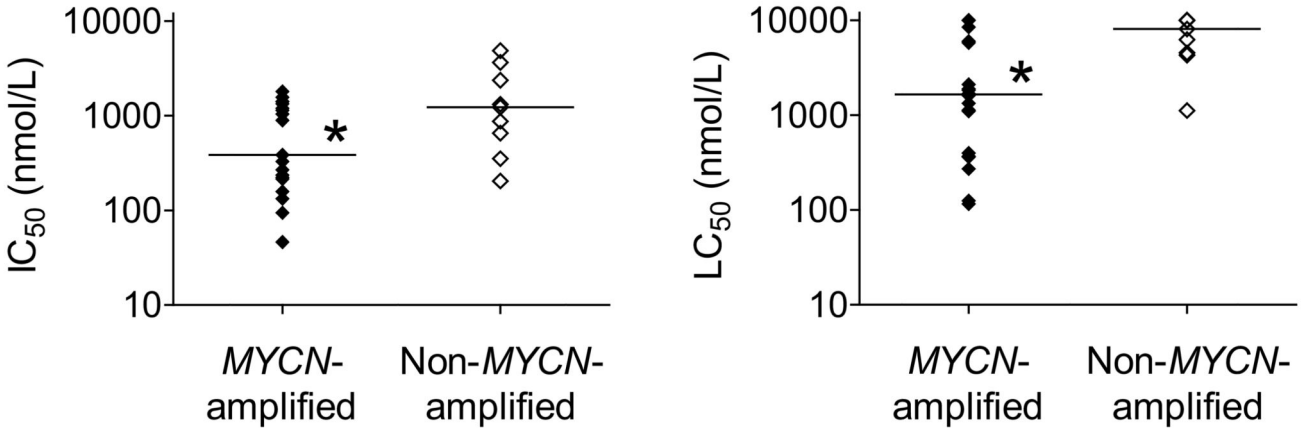

Figure 1.

MYCN-amplified neuroblastoma cells are more sensitive to AT7519 than non-*MYCN*-amplified neuroblastoma cells. IC_{50} (left) and LC_{50} values (right) of AT7519 were determined for 20 *MYCN*-amplified and 9 non-*MYCN*-amplified neuroblastoma cell lines. The lower values observed for *MYCN*-amplified neuroblastoma cells showed that these cells are more sensitive to AT7519. Statistical analysis was performed using one-tailed unpaired Student's t-test, with $P < 0.05$ (indicated as *) as the minimum level of significance. Horizontal lines indicate median values.

Europe PMC Funders Author Manuscripts

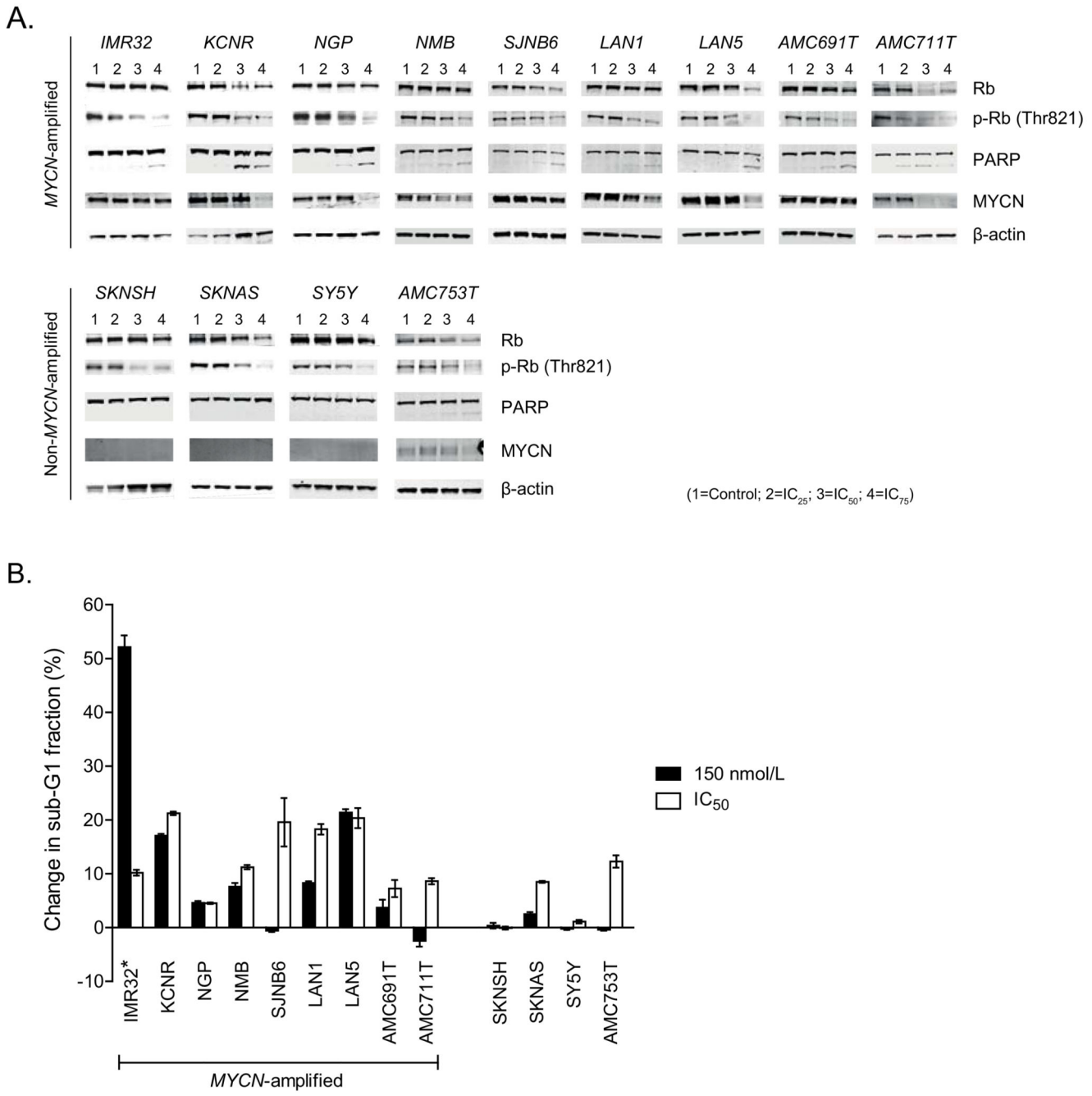

Figure 2.

AT7519 causes a more pronounced apoptotic response in *MYCN*-amplified neuroblastoma cells. A, Western Blot analysis of the *in vitro* effects of AT7519 on Rb phosphorylation, PARP cleavage and MYCN protein expression after 48 h treatment with concentrations equal to the IC_{25}, IC_{50} or IC_{75} for each individual cell line (IC_{25}, IC_{50} and IC_{75} values are specified in Supplementary Table S1). β-actin was used as household protein. Because of the limited expression of β-actin in neuroblastoma cell line SJNB6, α-tubulin was used as household protein for SJNB6. B, FACS analysis of the *in vitro* effects of AT7519 on sub-G1

induction after 72 h treatment. *As 72 h treatment of IMR32 cells with 150 nmol/L AT7519 resulted in complete cell degradation, IMR32 cells were treated with 100 nmol/L instead of 150 nmol/L AT7519.

Europe PMC Funders Author Manuscripts

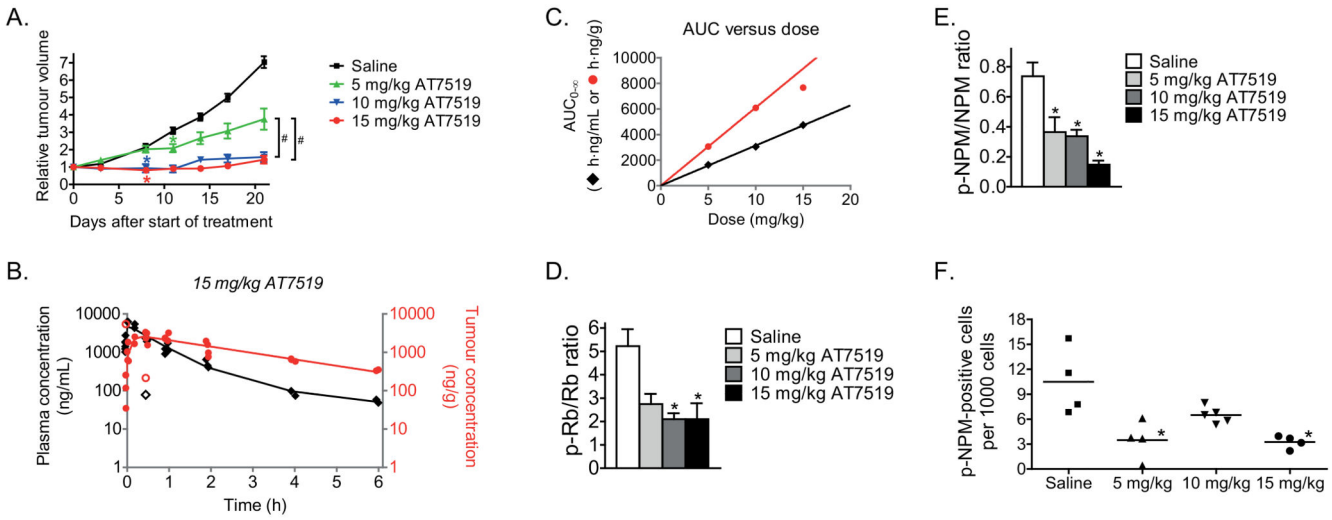

Figure 3.

Loss of Rb and NPM phosphorylation are biomarkers for the inhibitory effects of AT7519 on the growth of *MYCN*-amplified AMC711T neuroblastoma xenografts in mice. A, inhibitory effects of AT7519 on the growth of AMC711T neuroblastoma xenografts in mice. Relative tumour volume was calculated as the volume at the indicated day after start of treatment divided by the volume prior to treatment initiation. Data represent the mean relative tumour volume +/− S.E.M. (Group sizes: n = 10 (saline), n = 8 (5 mg/kg), n = 8 (10 mg/kg) and n = 11 (15 mg/kg)). Statistical differences between AT7519 treated and saline treated groups are indicated on the first day after treatment initiation at which a statistically different effect was observed (*). Statistical differences between the different doses AT7519 are indicated as #. B, plasma and intratumoural drug levels after administration of a single i.p. injection of 15 mg/kg AT7519 to mice bearing *MYCN*-amplified AMC711T neuroblastoma xenografts. Plasma AT7519 concentrations established at 1 min after administration have been averaged for curve fitting. Each symbol represents a single data point (tumour, solid red circles; plasma, solid black diamonds) and continuous lines represent the fitted curves. Outliers were calculated using Dixon's Q-test at a 95% confidence level. One tumour sample (i.e. 214.3 ng/g AT7519 at 0.5 h after administration) has been considered outlier based on corresponding plasma levels. Outliers are indicated by unfilled red circles for tumour samples and unfilled black diamonds for plasma samples. C, *in vivo* correlation between drug exposure ($AUC_{0-\infty}$) and AT7519 dose (tumour, red circles; plasma, black diamonds). D and E, *in vivo* inhibitory effects of AT7519 on the tumour phosphorylation states of the CDK2 targets Rb (D) and NPM (E). Phosphorylation states have been expressed as the ratio between phosphorylated and non-phosphorylated protein levels. β-actin was used as household protein. Data represent mean values +/− S.E.M. (n = 4 per group). F, *in vivo* inhibitory effects of AT7519 on phosphorylated NPM levels were confirmed by immunohistochemistry. Quantification was performed by manual counting of the number of p-NPM-positive cells in 40 microscopic fields per mouse sample at 40× magnification. The total cell number per field was estimated from hematoxylin-eosin stained tumour sections. Each symbol in the graph represents the average number of p-NPM-positive cells per 1000 cells for each individual mouse.

All statistical differences were calculated using one-way analysis of variance (ANOVA) Bonferroni adjustment and are indicated as *, unless stated otherwise. *P*-values < 0.05 were considered significant.

Europe PMC Funders Author Manuscripts

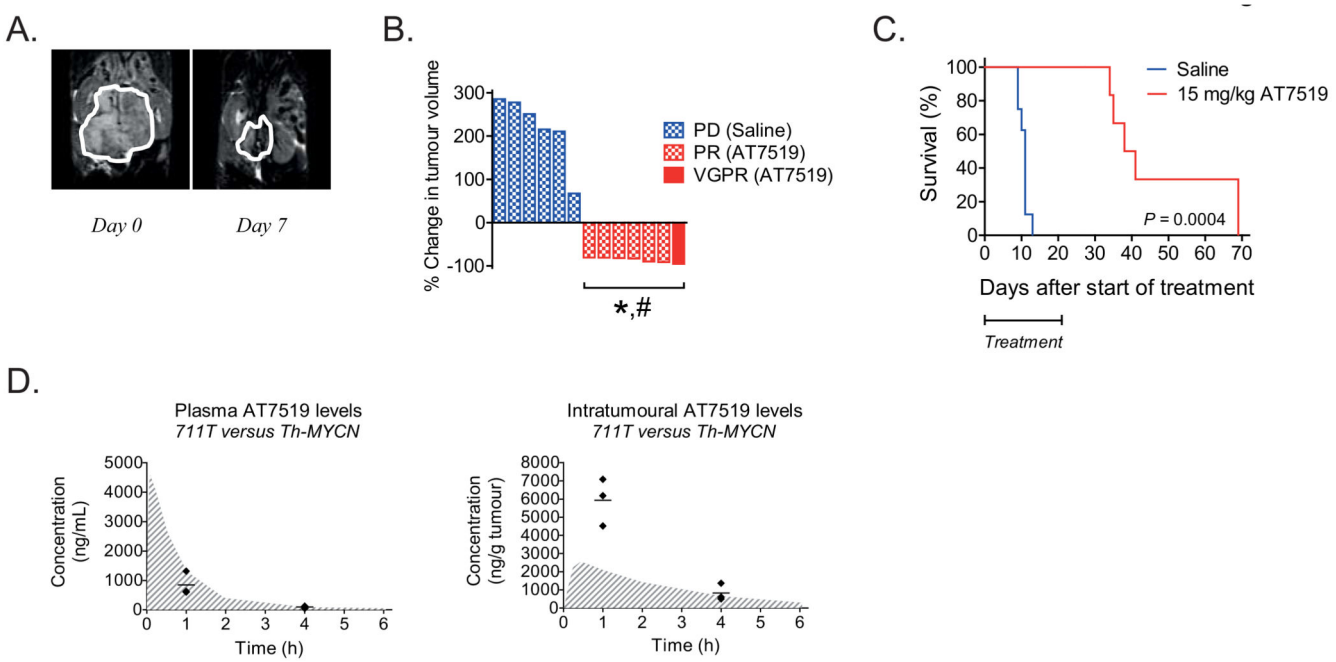

Figure 4.

AT7519 causes tumour volume reduction in *Th-MYCN* transgenic mice and improves overall survival. A, representative anatomical T2-weighted coronal MRI images for one of the AT7519-treated mice, showing the tumour prior to treatment (day 0; left) and at day 7 after treatment initiation (right). B, waterfall plot of the *in vivo* effects of AT7519 on tumour volume in *Th-MYCN* transgenic mice. The waterfall plot displays the % change in tumour volume at day 7 after treatment initiation for each individual mouse. Blue and white block bars represent the saline treated mice. The red bar and red and white block bars represent the mice treated with 15 mg/kg AT7519. PD = Progressive disease, PR = partial response (i.e. 50-95% tumour volume reduction) and VGPR = very good partial response (i.e. 95-99.99% tumour volume reduction). Statistical differences between the tumour size before and after treatment were calculated using one-tailed paired Student's t-test and are indicated as #. Statistical differences between the AT7519 treated and saline treated group were calculated using one-tailed unpaired Student's t-test and are indicated as *. *P*-values < 0.05 were considered significant. C, Kaplan-Meier curve to show the long-term survival after three weeks treatment with saline (n = 8; blue line) or AT7519 (n = 6; red line). Statistical analysis was performed using the Logrank (Mantel-Cox) test, with $P < 0.05$ as the minimum level of significance. D, comparison between plasma (left) and intratumoural (right) drug levels obtained in *Th-MYCN* transgenic mice and the AMC711T neuroblastoma xenograft model after administration of a single i.p. injection of 15 mg/kg AT7519. Gray and white line print areas in both graphs show again the fitted curves for the AMC711T neuroblastoma xenograft model. For the *Th-MYCN* transgenic mice, drug levels were established at 1 h and 4 h after administration of AT7519 (n = 3 per group) and individual data points (◆) as well as average drug levels (—) are shown in the graphs.

Europe PMC Funders Author Manuscripts

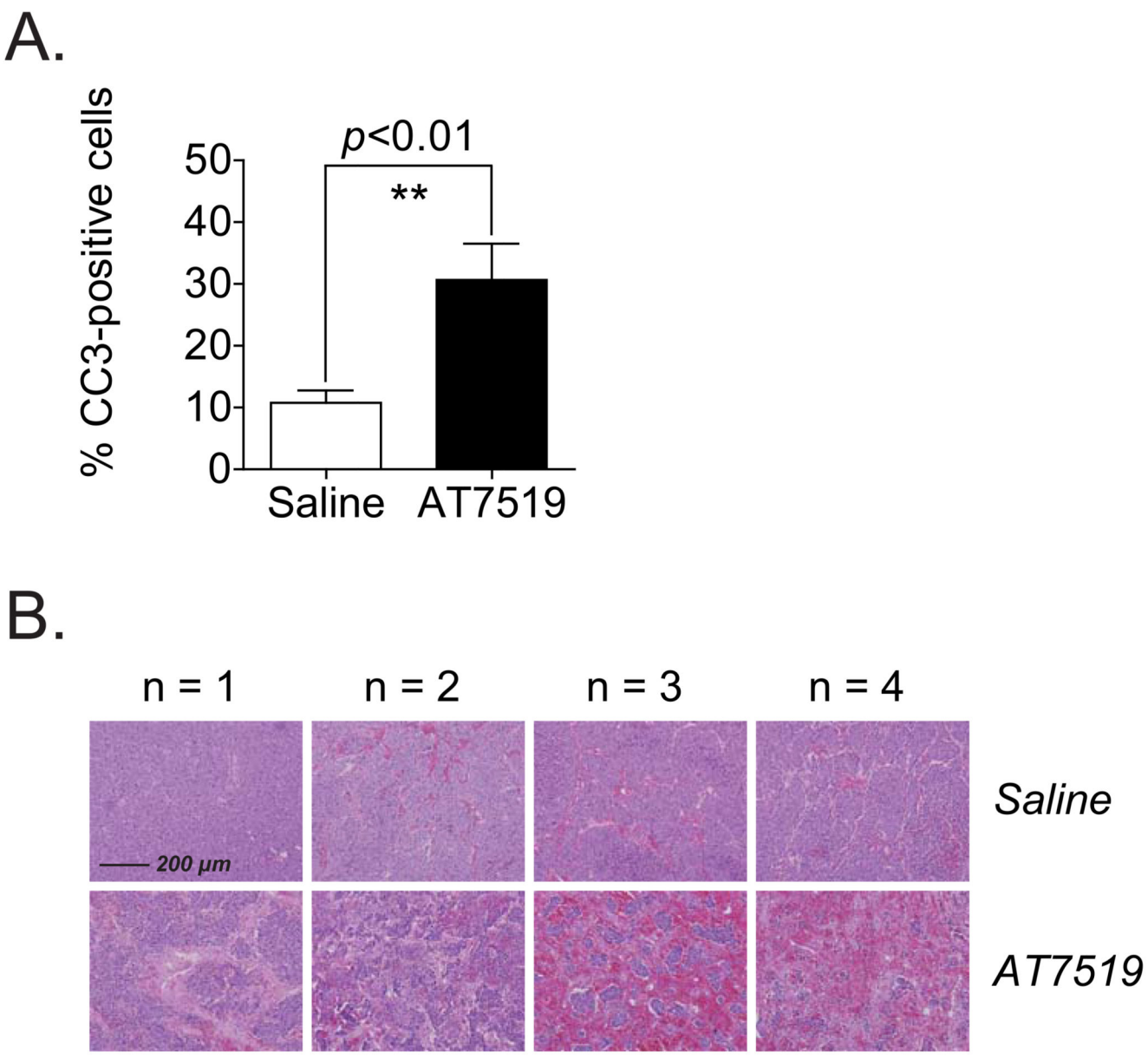

Figure 5.

AT7519 treatment of *Th-MYCN* transgenic mice results in massive apoptosis. *Th-MYCN* transgenic mice were treated with a daily i.p. injection of saline or 15 mg/kg AT7519 (n = 4 per group) for five consecutive days. At 6 h after administration of the last dose, tumour samples were collected for immunohistochemistry analysis of cleaved caspase 3 and hematoxylin-eosin staining. A, stimulatory effect of AT7519 on the pro-apoptotic marker cleaved caspase 3. Quantification was performed by manual counting of the total number of cells and the number of cleaved caspase 3-positive cells in 10 microscopic fields per mouse sample at 40× magnification (30% of each field). The average percentage of cleaved caspase 3-positive cells for each mouse was used to study the inducible effect of AT7519. Statistical differences between the AT7519 treated and saline treated group were calculated using one-

tailed unpaired Student's t-test and are indicated as ** ($P < 0.01$). B, representative microscopic images of hematoxylin-eosin stained paraffin-embedded tumour sections of saline treated and AT7519 treated mice (n = 4 per group). Magnification of the images: 10×. Scale bar: 200 μm.

Europe PMC Funders Author Manuscripts